Regularized Reconstruction to Reduce Blocking Artifacts of Block Discrete Cosine Transform Compressed Images

Yongyi Yang, Nikolas P. Galatsanos, *Member, IEEE,* and Aggelos K. Katsaggelos, *Senior Member, IEEE*

Abstract—**The block discrete cosine transform (BDCT) is by far the most widely used transform for the compression of both still and sequences of images. High compression ratios are usually achieved by discarding information about the BDCT coefficients that is considered unimportant and yield images that exhibit the visually annoying blocking artifact. In this paper reconstruction of images from incomplete BDCT data is examined. The problem is formulated as one of regularized image recovery. According to this formulation, the image in the decoder is reconstructed by using not only the transmitted data but also prior knowledge about the smoothness of the original image, which complements the transmitted data. Two methods are proposed for solving this regularized recovery problem. The first is based on the theory of projections onto convex sets (POCS) while the second is based on the constrained least squares (CLS) approach. For the POCS-based method, a new constraint set is defined that conveys smoothness information not captured by the transmitted BDCT coefficients, and the projection onto it is computed. For the CLS method an objective function is proposed that captures the smoothness properties of the original image. Iterative algorithms are introduced for its minimization. Experimental results are presented that demonstrate that with the regularized reconstruction it is possible to drastically reduce the blocking artifact and improve the performance using both subjective and objective metrics of traditional decoders, which use the transmitted BDCT coefficients only.**

I. Motivation and Introduction

IMAGE data compression is a very important problem for many emerging applications in the fields of visual communication and communication networks. Among the many available image compression approaches, transform-based methods are the most popular and have found many applications. The discrete cosine transform (DCT) is by far the most popular and widely used transform for image compression applications. Several desirable properties made DCT so popular. First, it exhibits very good energy compaction and decorrelation properties. It has been shown that the DCT is an asymptotic approximation to the optimal Karhunen–Loeve transform when the statistical properties of the image can be described by a first-order Markov model [5]. Furthermore, it has been demonstrated that most images encountered in visual communication applications are modeled extremely well by first-order Markov models [5]. Second, the DCT can be computed very efficiently using fast algorithms similar in nature to the well-known fast Fourier transform (FFT) [15].

Because of these properties the DCT has been recommended by both the Joint Photography Experts Group (JPEG) and the Motion Pictures Experts Group (MPEG) for compression of still and sequences of motion images, respectively. According to the JPEG and MPEG recommendations, the DCT is computed over a number of spatially partitioned regions (typically 16×16 or 8×8) called blocks [1], [15]. For the rest of this paper we shall refer to this block-by-block DCT of the image as the block-DCT (BDCT). This block partitioning takes advantage of the local spatial correlation properties of images and facilitates the VLSI hardware implementation of the DCT [5].

In transform-based image coders–decoders (codecs), in order to achieve high compression ratios, the process of generating the data to be transmitted to the decoder can be divided into two separate steps. First, after the data has been decorrelated by a suitable transformation, information that is not considered important about the transform coefficients is discarded. This is called irrelevancy reduction [11] and is an irreversible process that results in the degradation of the coded image. For the BDCT case, irrelevancy reduction is achieved by not transmitting and/or representing with less accuracy (quantizing) certain high-frequency coefficients [15], [3]. Second, the statistical redundancy of the data that has been decided upon for transmission to the decoder is removed using entropy encoding. This process is often called redundancy

Manuscript received November 12, 1992; revised July 5, 1993. The work of Y. Yang and N. Galatsanos was supported by Motorola. Paper was recommended by William B. Pennebaker.

Y. Yang and N. P. Galatsanos are with the Department of Electrical and Computer Engineering, Illinois Institute of Technology, Chicago, IL 60616.

A. K. Katsaggelos is with the Department of Electrical Engineering and Computer Science, Robert R. McCormick School of Engineering and Applied Science, Northwestern University, Evanston, IL 60208.

IEEE Log Number 9212198.

reduction and it is a reversible process that does not introduce any degradation [11]. In the decoder the received entropy encoded data are first decoded. Then, in order to keep the cost of the decoder low and to allow for real time compression of video sequences, the reconstruction algorithm used in most decoders until now is very simple. The coded image is reconstructed directly by the inverse BDCT using only the transmitted BDCT coefficients and setting the rest to zero.

It is well known in both the academic and industrial image processing communities that at high compression ratios reconstruction from partial BDCT information results in low-quality images. More specifically, the most noticeable artifact that these images exhibit is the blocking artifact. This artifact manifests itself as an artificial boundary among the pixels of adjacent blocks and constitutes a serious bottleneck for many important visual communication applications that require codecs that can yield visually pleasing images at very high compression ratios. The recent progress in VLSI technology makes us believe that inexpensive decoders that will implement sophisticated recovery algorithms in real time is a realistic expectation for the near future. Therefore, the incorporation of recovery algorithms at the decoders is a very promising approach to bridging the conflicting requirements of high-quality images and high compression ratios.

Limited efforts to address the problem described above have appeared in the literature. In [14] and [16] filtering the block borders is proposed. In [28] the problem of reconstructing better images from BDCT transform data is implicitly formulated as an image recovery problem, and the theory of projections onto convex sets (POCS) [26], [27] is invoked to justify the convergence of the proposed iterative algorithm. However, the smoothing operation used is not rigorously shown to be a projection onto a convex set, and therefore the convergence of the proposed algorithm can not be rigorously justified. The idea of using the theory of POCS for image sequence compression applications was first introduced in [18]. There, a novel compression scheme was proposed where convex sets were used instead of the basis functions of a transform coder. More recently, maximum a posteriori (MAP) reconstructions of the BDCT compressed images have been developed [13], [21].

In this paper the reconstruction of BDCT compressed images is formulated as a regularized image recovery problem. This work evolved from our initial work in [17]. Regularization is a general approach used in ill-posed recovery problems [25]. According to this approach the reconstruction is based on both the observed data and the prior knowledge that complements the available data. For the application under consideration, since reconstruction only from the available BDCT coefficients yields the blocking artifact, prior knowledge about the between-block smoothness must be used in the recovery algorithm.

Two methods are proposed to formulate and solve this regularized recovery problem; they are based on the theories of POCS [26], [27] and constrained least squares (CLS) [4]. For the POCS method, a new constraint set is defined that captures the between-block smoothness. The convexity of this set is shown and the projection onto it is computed. Thus, the reconstructed image is obtained by alternating projections onto the smoothness set and the set defined by the available partial information about the BDCT coefficients. For the CLS method, an objective function is introduced that incorporates into the recovery process both requirements, i.e., fidelity to the available information about the BDCT coefficients and smoothness. The smoothness properties of the image are captured by the regularization operator. The tradeoff between the conflicting requirements of fidelity to the available data and smoothness is controlled by the regularization parameter. Experimental results using test images are presented, which demonstrate the validity of both methods for the solution of this problem. The recovered images using both approaches are almost free from blocking artifacts and are superior to the images reconstructed from only the available BDCT coefficients based on both subjective and objective metrics.

The rest of this paper is organized as follows. In Section II the definition of the recovery problem is introduced. In Section III, POCS-based recovery is introduced and the detailed development of an algorithm using the theory of POCS is presented. In Section IV, the formulation and the resulting algorithm based on the theory of CLS are presented. In Section V experimental results are provided. Finally, in Section VI we present our conclusions and suggestions for future research.

II. Mathematical Definition of the Recovery Problem

Throughout this paper we will use the following conventions: Every real $N \times N$ image f is treated as an $N^2 \times 1$ vector in the space R^{N^2} by lexicographic ordering by either rows or columns. The BDCT is viewed as a linear transformation from R^{N^2} to R^{N^2}. Then, for an image f we can write

$$F = Bf, \quad \text{and} \quad f = B^t F, \tag{1}$$

where F is the BDCT of f and B is the BDCT matrix. Matrix B for an $N \times N$ image that is divided into $M \times M$ blocks is a $N^2 \times N^2$ block-diagonal matrix with $\left(\frac{N}{M}\right)^2$ matrixes of size $M^2 \times M^2$ along the diagonal. These $M^2 \times M^2$ DCT matrixes along the diagonal of B are identical and their explicit expression is well known (see [15], for example). Due to the unitary property of the DCT matrices, the BDCT matrix is also unitary and the inverse transform can be simply expressed by B^t, where t denotes the transpose of a vector or matrix.

The elements of F in (1) are the expression coefficients of the vector f using the BDCT basis in R^{N^2}. That is, f can be written as

$$f = \sum_{n=1}^{N^2} F_n e_n \tag{2}$$

where $\boldsymbol{e}_n$ denotes the normalized BDCT basis vectors and F_n is the BDCT coefficient of $\boldsymbol{f}$.

In image compression, only a fraction of the BDCT coefficients are coded and transmitted to the decoder. Let $\mathcal{I}$ be the set of indices of the transmitted BDCT coefficients. Then (2) can be rewritten as

$$\boldsymbol{f} = \sum_{n \in \mathcal{I}} F_n \boldsymbol{e}_n + \sum_{n \notin \mathcal{I}} F_n \boldsymbol{e}_n. \tag{3}$$

Let $\mathcal{Q}$ denote the quantization operator used in the coder; then in the decoder we have available the quantized BDCT coefficients $\{F'_n;\ n \in \mathcal{I}\}$, where $F'_n = \mathcal{Q}[F_n]$. In the decoder the coded image is reconstructed by assuming the nontransmitted BDCT coefficients $\{F'_n s,\ n \notin \mathcal{I}\}$ are equal to 0. Thus the reconstructed image is given by

$$\boldsymbol{f}' = \sum_{n \in \mathcal{I}} F'_n \boldsymbol{e}_n \tag{4}$$

which as explained earlier exhibits the visually annoying blocking artifact.

Using the previous notation, our goal in this paper is to compute estimates of both sets of coefficients $\{F_n;\ n \notin \mathcal{I}\}$ and $\{F_n;\ n \in \mathcal{I}\}$. The information used for this task is the transmitted coefficients $\{F'_n;\ n \in \mathcal{I}\}$, knowledge of the quantization operator $\mathcal{Q}$, and prior knowledge about the smoothness properties of the original image. The set $\mathcal{I}$ of the transmitted BDCT coefficients and the quantizer $\mathcal{Q}$ depends on the irrelevancy reduction method used [11].

III. Regularized Image Recovery Using the Theory of Projections onto Convex Sets (POCS)

In this section we first briefly review the basic results of POCS theory, and then we present in detail their application to our problem.

A. Brief Review of the POCS Theory

The theory of POCS was introduced to the engineering image processing community by Youla's work in [26] and [27]. Since then, this theory has found many applications in various image recovery problems [20], [9]. Assume that all images $\boldsymbol{f}$, represented as $N^2 \times 1$ vectors, are elements of a Hilbert space H. Then, for any vector $\boldsymbol{f} \in H$, its projection $P\boldsymbol{f}$ onto a closed convex set $C \subset H$ is defined as the closest element to $\boldsymbol{f}$ in C, i.e.,

$$\|\boldsymbol{f} - P\boldsymbol{f}\| = \min_{\boldsymbol{g} \in C} \|\boldsymbol{f} - \boldsymbol{g}\|.$$

It is well known that $P\boldsymbol{f}$ is uniquely determined by $\boldsymbol{f}$ and C.

Assume now that m closed convex sets C_i, $i = 1, 2, \cdots, m$, in H, are available and that P_i is the projector onto C_i for $i = 1, 2, \cdots, m$. It was shown that for any arbitrary initial vector $\boldsymbol{f}_0$, the sequence of vectors $\{\boldsymbol{f}_k\}$ generated by the iteration

$$\boldsymbol{f}_{k+1} = T_m T_{m-1} \cdots T_1 \boldsymbol{f}_k \tag{5}$$

where $T_i = I + \lambda_i (P_i - I)$, $0 < \lambda_i < 2$, $i = 1, 2, \cdots, m$, converges to a point

$$\boldsymbol{f}^* \in C_0 \triangleq \bigcap_{i=1}^{m} C_i.$$

The key idea for the application of the theory of POCS to image recovery problems is to represent every known property of the original image by a closed convex set. Therefore, for m known properties, there are m closed convex sets C_i. Then, a vector $\boldsymbol{f}^*$, common to all sets C_i, $i = 1, 2, \cdots, m$, can be found by alternating projections onto each one of them, starting from any initial guess vector. Clearly, the point of convergence $\boldsymbol{f}^*$ possesses all the m desired properties of the original image.

B. POCS-Based Regularized Recovery: Convex Constraint Sets and their Projectors

It is clear from the discussion in Section III-A that the definition of a POCS-based recovery algorithm requires two things. First, the definition of the closed convex constraint sets that represent all the available knowledge about the original image, and second, the computation of the projections onto these sets. Furthermore, based on the principle of regularization, two types of constraint are necessary: the constraint set(s) with the information captured by the available data and the constraint set(s) with the prior knowledge that is introduced to complement the available data. More specifically, these constraint sets are as follows: constraint sets that capture the knowledge available about the BDCT coefficients in the decoder, and constraint sets that capture the smoothness properties of the desired image.

The set C'_1, which is based on the known BDCT coefficients, is defined by

$$C'_1 \triangleq \{\boldsymbol{f}: (\mathcal{Q}B\boldsymbol{f})_n = F'_n, \forall n \in \mathcal{I}\} \tag{6}$$

where B, $\mathcal{Q}$, F'_n, and $\mathcal{I}$ were defined previously. In general, C'_1 is not a closed set. Instead C_1 the closure of C'_1 is used. This set is given by

$$C_1 = \{\boldsymbol{f}: F_n^{\min} \le (B\boldsymbol{f})_n \le F_n^{\max}, \forall n \in \mathcal{I}\} \tag{7}$$

where $F_n^{\min}$ and $F_n^{\max}$ are determined by the quantizer used. By definition, C_1 is a constraint set that captures all known information about the received BDCT coefficients. It is easy to show that C_1 is closed and convex. The projection $P_1\boldsymbol{f}$ of an arbitrary vector $\boldsymbol{f}$ in R^{N^2} onto C_1 is given by [20] and [28]:

$$P_1\boldsymbol{f} = B^t \cdot \boldsymbol{F} \tag{8}$$

where B^t is defined in (1) and $\boldsymbol{F}$ is determined by

$$F_n = \begin{cases} F_n^{\min} & \text{if } (B\boldsymbol{f})_n < F_n^{\min} \\ F_n^{\max} & \text{if } (B\boldsymbol{f})_n > F_n^{\max} \\ (B\boldsymbol{f})_n & \text{if } F_n^{\min} \le (B\boldsymbol{f})_n \le F_n^{\max}. \end{cases} \qquad 1 \le n \le N^2,\ n \in \mathcal{I} \tag{9}$$

Constraint sets that capture the continuity between block boundaries contain information that is *lost*, when only the transmitted BDCT coefficients are used for reconstruction. Thus, information about smoothness in the block boundaries *complements* the information conveyed by the BDCT coefficients and is very important for this reconstruction problem. For this purpose, two new constraint sets C_2 and C_2' are defined.

For the definition of the set C_2, the $N \times N$ image f is represented in column vector form as

$$f = \{f_1, f_2, \cdots, f_N\}, \tag{10}$$

where f_i denotes the ith column of the image. Let Q be a linear operator such that Qf represents the difference between the columns at the block boundaries of the image f. For example, for the case of $N = 512$ and 8×8 blocks,

$$Qf = \begin{bmatrix} f_8 - f_9 \\ f_{16} - f_{17} \\ \vdots \\ f_{504} - f_{505} \end{bmatrix}. \tag{11}$$

The norm of Qf

$$\|Qf\| = \left[\sum_{i=1}^{63} \|f_{8\cdot i} - f_{8\cdot i+1}\|^2 \right]^{\frac{1}{2}} \tag{12}$$

is the total intensity variation between the boundary columns of adjacent blocks.

Set C_2 is defined by

$$C_2 \triangleq \{f : \|Qf\| \le E\} \tag{13}$$

where E is the scalar upper bound that defines the size of this set. The choice of E is discussed in detail in Sections V and VI. It is easy to see that set C_2 is an ellipsoid that is both closed and convex. C_2 was one of the ellipsoids used in [7] and [8] for obtaining solutions to the image restoration problem.

For an image $f \in R^{N^2}$ in column form $\{f_1, f_2, \cdots, f_N\}$, its projection $\tilde{f} = P_2 f$ onto set C_2 is represented in column form by $\{\tilde{f}_1, \tilde{f}_2, \cdots, \tilde{f}_N\}$. In Appendix A we show that for a 512×512 image and 8×8 blocks

$$\begin{aligned} \tilde{f}_i &= \alpha \cdot f_i + (1 - \alpha) \cdot f_{i+1} \\ \text{and} \quad \tilde{f}_{i+1} &= (1 - \alpha) \cdot f_i + \alpha \cdot f_{i+1} \\ &\text{for } i = 8 \cdot k \quad \text{and} \quad k = 1, 2, \cdots, 63; \\ \text{otherwise,} \quad \tilde{f}_i &= f_i, \end{aligned} \tag{14}$$

where $\alpha = \frac{1}{2}\left[\frac{E}{\|Q \cdot f\|} + 1\right]$. This result can be generalized in a straightforward manner for any image and block sizes. Set C_2 captures the intensity variations between the columns of the block boundaries of an image. In a similar fashion, we can also define the set C_2', which captures the intensity variations between the rows of the block boundaries. The projector P_2' onto C_2' can be found in the same fashion as P_2. Note that sets C_2 and C_2' capture only the variations between the columns and rows at block boundaries. We can also define similar smoothness constraint sets for adjacent columns and rows off the block boundaries. These sets are called off-block boundary smoothness sets.

It is worth noting that set C_2 defined in (13) can be generalized for any linear operator Q. The projector in this case is given by [22], [7], [24]

$$Pf = (I + \lambda Q^t Q)^{-1} f \tag{15}$$

where the Lagrange multiplier λ depends on E and Q and is found such that the bound in (13) is satisfied with equality. If Q is a high-pass operator, this set represents also a smoothness constraint. However, in general P is difficult to compute since the computation of λ requires the numerical solution of a nonlinear equation. In contrast, the computation of P_2 and P_2' is straightforward.

Using the previously defined sets C_1, C_2, and C_2', the resulting POCS-based recovery algorithm can be described by the following steps:

1) Take $f_0 = f'$ the initial guess.
2) For $k = 1, 2, \cdots$, compute f_k according to
$$f_k = P_2' P_2 P_1 f_{k-1} \tag{16}$$
where P_i and P_i' are the projectors onto sets C_i and C_i', respectively.
3) Continue iterating until $\|f_k - f_{k-1}\|$ is less than some prescribed bound.

Note that (16) is general and can incorporate other constraint sets, such as off-block boundary smoothness and positivity.

IV. Constrained Least Squares (CLS) Regularized Recovery

A. Mathematical Preliminaries

In this section we describe the development of another regularized recovery approach, which is based on the theory of CLS [4]. Before going into the details of this approach, let us adopt some notations. For an image vector $f \in R^{N^2}$ with F as its BDCT coefficient vector, we define the diagonal matrix I_c such that

$$(I_c F)_n \triangleq \begin{cases} F_n & \text{if } n \in \mathcal{S} \\ 0 & \text{otherwise} \end{cases}$$

where $\mathcal{S}$ is the set of transmitted BDCT coefficients that was defined earlier. We also define the matrix $\bar{I}_c$ as

$$\bar{I}_c \triangleq I - I_c$$

where I is the identity operator.

By definition, I_c selects the BDCT coefficients that are transmitted to the decoder, while $\bar{I}_c$ selects the ones that are not. It is easy to show that both matrixes are idempotent, i.e.,

$$I_c \cdot I_c = I_c \quad \text{and} \quad \bar{I}_c \cdot \bar{I}_c = \bar{I}_c \tag{17}$$

and also

$$I_c \cdot \bar{I}_c = \bar{I}_c \cdot I_c = 0 \tag{18}$$

B. Regularized Recovery Using CLS: Objective Function and Minimization Algorithms

The CLS approach has been used successfully in many regularized image recovery problems (see for example [4], [6], [8]–[10], and [2]). According to this approach, the recovered image is obtained by minimizing an objective function, which is the weighted sum of two functions that impose conflicting requirements on the recovered image. Thus, if one of these functions penalizes deviation from the available data the other must penalize the undesired effects if an image is reconstructed only from the available data. In this sense, the second function introduces prior knowledge that complements the available data or, in other words, constrains the behavior of the reconstructed image.

For the reconstruction of the image from partial knowledge of the BDCT coefficients we propose the minimization of the following function with respect to f:

$$J_\mu \triangleq \|Sf\|^2 + \mu\|f - f'\|^2 = J_S + \mu J_D \tag{19}$$

where $\|\cdot\|$ is the usual l_2 norm, μ is a nonnegative scalar called the regularization parameter, f' is the blocky image that is reconstructed from the transmitted data defined in (4), and operator S is called the regularization operator [25].

For S a high-pass operator, J_S is a measure of the local variation of f. In other words, J_S is a smoothness measure for f and is minimized by a constant image, the possible smoothest image. On the other hand, J_D is a distance measure between the image f and the blocky image f' and is minimized by f'. Thus, J_S and J_D complement each other, as required by the theory of regularization. The regularization parameter μ is used to define the tradeoff between the smoothness and the fidelity to the data in the final solution.

In what follows we present two approaches of the CLS regularization algorithm. According to the first, we assume that the quantizer used at the coder is not known at the decoder. Thus, only the unsent BDCT coefficients $\bar{I}_c\boldsymbol{F}$ are estimated. According to the second, we assume that the quantizer used at the coder is known by the decoder. Thus the entire array of BDCT coefficients $\boldsymbol{F}$ is estimated incorporating the knowledge of the quantizer in the recovery algorithm. The attractive feature of the first approach is that it yields a linear algorithm that is mathematically tractable and offers valuable insight into the behavior of the recovered image f.

1) Estimating $\bar{I}_c\boldsymbol{F}$: The BDCT Coefficients that are not Transmitted: Based on the introduction of I_c and $\bar{I}_c$, (1) is rewritten as

$$f = B^t\left(I_c + \bar{I}_c\right)\boldsymbol{F} = B^tI_c\boldsymbol{F} + B^t\bar{I}_c\boldsymbol{F}.$$

This is the vector form of (3). Note that for this version of the CLS approach we assume $I_c\boldsymbol{F} = Bf'$, and thus, for each image vector f,

$$f = f' + B^t\bar{I}_c\boldsymbol{F}. \tag{20}$$

Therefore, we have

$$J_S = \|Sf' + SB^t\bar{I}_c\boldsymbol{F}\|^2 \tag{21}$$

and

$$J_D = \|B^t\bar{I}_c\boldsymbol{F}\|^2 = \|\bar{I}_c\boldsymbol{F}\|^2. \tag{22}$$

As explained previously for this version of the regularized CLS reconstruction, our objective is the recovery of $\bar{I}_c\boldsymbol{F}$ only. The gradient of J_μ with respect to $\boldsymbol{F}$ is equal to

$$\nabla J_\mu = 2\bar{I}_cBS^tS\left(f' + B^t\bar{I}_c\boldsymbol{F}\right) + 2\mu\bar{I}_c\boldsymbol{F}. \tag{23}$$

Because of the convexity of J_μ this functional is minimized when $\nabla J_\mu = 0$. This yields

$$\left(\mu I + \bar{I}_cBS^tSB^t\right)\bar{I}_c\boldsymbol{F} = -\bar{I}_cBS^tSf'. \tag{24}$$

The idempotent property of the matrix $\bar{I}_c$ combined with (24) yields

$$\left(\mu I + \bar{I}_cBS^tSB^t\bar{I}_c\right)\bar{I}_c\boldsymbol{F} = -\bar{I}_cBS^tSf'. \tag{25}$$

With

$$A_{(\mu)} \triangleq \mu I + \bar{I}_cBS^tSB^t\bar{I}_c \tag{26}$$

the regularized estimate of the missing BDCT coefficients can be obtained by solving the following equation:

$$A_{(\mu)}\bar{I}_c\boldsymbol{F} = -\bar{I}_cBS^tSf'. \tag{27}$$

Let $\lambda_1, \lambda_2, \cdots, \lambda_{N^2}$ denote the increasingly ordered eigenvalues of the positive semidefinite matrix $\bar{I}_cBS^tSB^t\bar{I}_c$, that is,

$$0 \le \lambda_1 \le \lambda_2 \le \cdots \le \lambda_{N^2} \le \|S^tS\|.$$

$A_{(\mu)}$, defined in (26), is strictly positive-definite if μ is positive. Furthermore, all its eigenvalues satisfy the following relation:

$$0 < \mu + \lambda_1 \le \mu + \lambda_2 \le \cdots \le \mu + \lambda_{N^2} \le \mu + \|S^tS\|. \tag{28}$$

Hence matrix $A_{(\mu)}$ is invertible, and (27) yields

$$\bar{I}_c\boldsymbol{F} = -A_{(\mu)}^{-1}\bar{I}_cBS^tSf'. \tag{29}$$

It follows from (20) that the recovered image can be written as

$$f = \left(I - B^tA_{(\mu)}^{-1}\bar{I}_cBS^tS\right)f'. \tag{30}$$

The direct computation of f in (30) is prohibitive even for moderate-size images, due to the required inversion of matrix $A_{(\mu)}$. However, the product of $A_{(\mu)}$ with any vector is easy to compute. Thus, we chose to find f iteratively using the successive approximation iteration [19], [6], [7], [8]. Applying $B^tA_{(\mu)}B$ to both sides of (30), we obtain

$$B^tA_{(\mu)}Bf = B^t\left(A_{(\mu)}B - \bar{I}_cBS^tS\right)f'. \tag{31}$$

Since both B and $A_{(\mu)}$ are invertible, (30) and (31) are equivalent. The successive approximation iteration for (31) is given by

$$\boldsymbol{f}_k = \boldsymbol{f}_{k-1} + cB^t(\boldsymbol{b} - A_{(\mu)}B\boldsymbol{f}_{k-1}) \tag{32}$$

where c is a nonzero scalar and $\boldsymbol{b} = (A_{(\mu)}B - \bar{I}_c BS^tS)\boldsymbol{f}'$. (32) can be further simplified in the following way. Applying B to both sides yields

$$\boldsymbol{F}_k = \boldsymbol{F}_{k-1} + c(\boldsymbol{b} - A_{(\mu)}\boldsymbol{F}_{k-1}) \tag{33}$$

where $\boldsymbol{F}_k$ is the BDCT of $\boldsymbol{f}_k$. (33) is equivalent to (32). However, the latter is computationally more efficient because multiplication by B^t is avoided. It is clear that a fixed point of iteration of (32) must satisfy (31). From the earlier discussion, matrix $A_{(\mu)}$ is positive-definite and well defined. Therefore, (30) has a unique solution. We show next that (33) has a unique fixed point and this fixed point represents our recovered image. From (33) we have

$$\boldsymbol{F}_{k+1} - \boldsymbol{F}_k = (I - cA_{(\mu)})(\boldsymbol{F}_k - \boldsymbol{F}_{k-1}). \tag{34}$$

Thus, the mapping defined by (33) is contractive and therefore iteration (33) has a unique fixed point if [12]

$$\|I - cA_{(\mu)}\| < 1. \tag{35}$$

Condition (35) is used to define the range of values of c. It can be further simplified by considering the eigenvalues of $A_{(\mu)}$. When c satisfies the relation

$$0 < c < \frac{2}{\mu + \|S^tS\|} \tag{36}$$

condition (35) is satisfied.

CLS-based regularized recovery requires the selection of the regularization parameter μ. This parameter balances the roughness measure J_S and difference measure J_D in the recovered image. It is instructive to examine the solution given by (30) for the two extreme choices of μ. First, when $\mu = 0$, the recovered image minimizes the smoothness measure directly. It is easy to see that it yields the smoothest image that satisfies the received BDCT coefficients. Second, when $\mu = \infty$, then $\bar{I}_c\boldsymbol{F} = 0$. Thus, the recovered image becomes the blocky image $\boldsymbol{f}'$.

The recovery problem examined in this paper has a differentiating feature from other image recovery problems in that the original image is *known* in the coder. Thus, unlike other recovery problems where the regularization parameter has to be chosen using the available data [2], in this problem it can be chosen using the original image. The approach we follow is to compute the ratio r of J_S and J_D when the original image is used and then find μ, which will match this ratio, that is, $\Psi_{(\mu)} = J_{S(\mu)}/J_{D(\mu)} = r$, where $J_{S(\mu)}$ and $J_{D(\mu)}$ are computed using the reconstructed image with a fixed value of μ.

Using (21) and (30), the roughness measure $J_{S(\mu)}$ of the recovered image can be written as

$$J_{S(\mu)} = \|S\boldsymbol{f}\|^2 = \left\| S\left(I - B^tA_{(\mu)}^{-1}\bar{I}_c BS^tS\right)\boldsymbol{f}'\right\|^2. \tag{37}$$

Similarly, from (22) and (29), the difference measure $J_{D(\mu)}$ is equal to

$$J_{D(\mu)} = \left\| A_{(\mu)}^{-1}\bar{I}_c BS^tS\boldsymbol{f}'\right\|^2. \tag{38}$$

In Appendix B we have shown the following two propositions:

Proposition 1: $J_{S(\mu)}$ is a strictly increasing function of μ.

Proposition 2: $J_{D(\mu)}$ is a strictly decreasing function of μ.

Based on the above two propositions, we conclude that as the regularization parameter μ varies from 0 to ∞, the recovered image changes continuously from the smoothest to the most blocky one, i.e., the image recovered directly from received BDCT coefficients. It is also clear that $\Psi_{(\mu)}$ is a strictly decreasing function of μ. In other words, as μ varies from 0 to ∞, the ratio $\Psi_{(\mu)}$ decreases continuously. Thus, we can always find one value of μ that matches the desired ratio r.

2) Estimating F: The Entire Array of BDCT Coefficients: As already explained, according to this approach, the entire array of BDCT coefficients $\boldsymbol{F}$ is estimated using $\boldsymbol{f}'$ as the data. The functional J_μ is minimized again with respect to $\boldsymbol{f}$ but unlike the previous case we solve for the entire array $\boldsymbol{f}$. This yields

$$\left(I + \frac{1}{\mu}S^tS\right)\boldsymbol{f} = \boldsymbol{f}' \tag{39}$$

where $\boldsymbol{f}'$ is the blocky image given in (4). Equation (39) can be written in the BDCT domain as

$$\left(I + \frac{1}{\mu}BS^tSB^t\right)\boldsymbol{F} = \boldsymbol{F}'. \tag{40}$$

Equation (40) can be solved using the iteration

$$\boldsymbol{F}_k = \boldsymbol{F}_{k-1} + c\left(\boldsymbol{F}' - \left(I + \frac{1}{\mu}BS^tSB^t\right)\boldsymbol{F}_{k-1}\right) \tag{41}$$

where c is chosen to satisfy

$$0 < c < \frac{2\mu}{\mu + \|S^tS\|} \tag{42}$$

to guarantee its convergence.

Since the real symmetric matrices S^tS and $(I + \frac{1}{\mu}S^tS)$ have the same eigenvectors, it is easy to show that

$$J_{S(\mu)} = \sum_{n=1}^{N^2}\left[\frac{s_n}{1 + \frac{1}{\mu}s_n}\right]^2\left(\hat{F}_n'\right)^2$$

$$\text{and} \quad J_{D(\mu)} = \sum_{n=1}^{N^2}\left[\frac{s_n}{\mu + s_n}\right]^2\left(\hat{F}_n'\right)^2 \tag{43}$$

where s_n, $n = 1, 2, \cdots, N^2$, are the eigenvalues of S^tS, which are nonnegative, $\hat{\boldsymbol{F}}' = W^t\boldsymbol{f}'$, and W is a unitary matrix formed by the eigenvectors of S^tS. Thus, again for this version of the regularized CLS algorithm, $J_{S(\mu)}$ and

$J_{D(\mu)}$ are strictly increasing and decreasing functions of μ, respectively. Therefore, the value of the regularization parameter can be computed again from the original image, as explained in the previous section.

If the quantizer used at the coder is known at the decoder, this knowledge can be incorporated in the recovery process by the modified iteration

$$\boldsymbol{F}_k = \tilde{\boldsymbol{F}}_{k-1} + c\left(\boldsymbol{B}\boldsymbol{f}' - \left(\boldsymbol{I} + \frac{1}{\mu}\boldsymbol{B}\boldsymbol{S}'\boldsymbol{S}\boldsymbol{B}'\right)\tilde{\boldsymbol{F}}_{k-1}\right), \quad (44)$$

$$\tilde{\boldsymbol{F}}_k = P_1\boldsymbol{F}_k \quad (45)$$

where P_1 is the projector onto the set C_1 defined by (8) and (9). Since P_1 is a projector onto a closed convex set, it is not expansive [26]. Thus, it can be shown that the iteration (45) converges and minimizes the functional J_μ on the closed convex set C_1 [10]. Therefore, the fixed point of iteration (45) yields the desired image.

V. Experiments

In this section experiments are presented to test the proposed algorithms. Both POCS- and CLS-based regularized reconstruction algorithms are tested. The 512 × 512 Lena image was used in our experiments. The center 256 × 256 section of this image is shown in Fig. 1. The same center section of the processed images will be shown in the following. This image was divided into 8 × 8 blocks, and the DCT of each block was taken to generate the BDCT coefficients. Two irrelevancy reduction methods were implemented to produce the data to be used by our regularized reconstruction algorithms. First, the irrelevancy reduction approach based on partition priority coding (PPC) in [3] was implemented. This method is based on thresholding, coefficients smaller than a selected threshold are set to zero, and the transmitted BDCT coefficients are uniformly quantized using 8 bits/coefficient. Second, the JPEG recommendation was implemented and quantization tables were used to determine the quantizer in the coder [1]. The two blocky images shown in Figs. 2 and 3 were obtained by PPC- and JPEG-based irrelevancy reduction, respectively. For the PPC approach the threshold was set to 48. For the JPEG approach the quantization table from [28] shown in Table I was used. As an objective measure of the distance between two images $\boldsymbol{g}$ and $\boldsymbol{h}$, we used the peak signal-to-noise ratio (PSNR). For $N \times N$ images with [0, 255] gray-level range PSNR is defined in dB by

$$\text{PSNR} = 10\log_{10}\left[\frac{N^2 \times 255^2}{\|\boldsymbol{g} - \boldsymbol{h}\|^2}\right]. \quad (46)$$

The PSNR of the blocky images obtained by PPC and JPEG irrelevancy reduction was 30.03 and 29.58 dB, respectively.

POCS-based regularized reconstruction was tested first. The upper bounds E and E' used to define sets C_2 and C_2' were determined using the blocky images. The blocky image $\boldsymbol{f}'$ written in column vector form is $\boldsymbol{f}' =$

Fig. 1. The original Lena image; the middle 256 × 256 section from the 512 × 512 image is shown.

Fig. 2. The blocky image obtained from PPC irrelevancy reduction; PSNR = 30.03 dB.

Fig. 3. The blocky image obtained from JPEG irrelevancy reduction; PSNR = 29.58 dB.

TABLE I
THE QUANTIZATION TABLE FROM [28] WAS USED FOR JPEG-BASED IRRELEVANCY REDUCTION

50	60	70	70	90	120	255	255
60	60	70	96	130	255	255	255
70	70	80	120	200	255	255	255
70	96	120	145	255	255	255	255
90	130	200	255	255	255	255	255
120	255	255	255	255	255	255	255
255	255	255	255	255	255	255	255
255	255	255	255	255	255	255	255

$\{f'_1, f'_2, \cdots, f'_{512}\}$. Then E was estimated from f' by

$$S_k \triangleq \left[\sum_{i=1}^{63} \|f'_{8\cdot i+k} - f'_{8\cdot i+k+1}\|^2\right]^{\frac{1}{2}},$$

$$E = \frac{1}{7}\sum_{k=1}^{7} S_k \quad \text{and} \quad k = 1, 2, \cdots, 7.$$

This E is a measure of the average vertical discontinuity between adjacent columns of the entire image and was found to yield satisfactory results when used as a bound for the set C_2. In a similar fashion the bound E' was obtained. The reconstructed images from the PPC- and JPEG-obtained blocky images are shown in Figs. 4 and 5, respectively. The corresponding PSNR's are equal to 30.91 and 30.30 dB.

The CLS approach was also tested. From the discussions in Section IV, the regularization approach requires the selection of the regularization parameter μ and operator S. For the selection of μ the original image was used as explained in section IV-B. For the selection of S, the following considerations were taken into account: a) S must be able to capture the blocking effects, i.e., the intensity discontinuities between the block boundaries, and b) the region of support of S should be small in order to prevent blurring the recovered image. We therefore chose S to be a high-pass convolutional filter generated by the mask s. The nonzero coefficients of s are $s(0,0) = 2$, $s(0,1) = -1$, and $s(1,0) = -1$.

For PPC-based irrelevancy reduction both versions of the CLS algorithm in (33) and (45) yield almost identical results. This is expected, since all transmitted BDCT coefficients are quantized very accurately with 8 b/coefficient. However, for JPEG-based irrelevancy reduction the two versions of the CLS algorithm yield different results. As expected, the second version that incorporates the knowledge of the quantizer into the algorithm results in considerably better results. In Fig. 6, the image resulting from the reconstruction of the PPC blocky image using (33) is shown. In Figs. 7 and 8, the recovered images resulting from reconstruction using the JPEG blocky image based on (33) and (45) are shown respectively. The PSNR's of the images in Figs. 6, 7, and 8 are 30.25, 29.68, and 29.65 dB, respectively. It is interesting to notice that although the image in Fig. 7 has ringing artifacts around its edges it has a higher PSNR than the visually more pleasing image in Fig. 8.

From its definition in (46), PSNR is a distance measure between two images. It is well known that PNSR does not always match the human perception for image quality. It is clear that in some of the previous experiments, though the blocking artifacts are drastically reduced, the difference in PSNR is not indicative of this improvement.

VI. Conclusions

In this paper regularized image recovery was applied to the problem of reconstructing images from partial BDCT data. This problem is encountered in most present image

Fig. 4. POCS recovery from the PPC blocky image; PSNR = 30.91 dB.

Fig. 5. POCS recovery from the JPEG blocky image; PSNR = 30.30 dB.

Fig. 6. CLS recovery from the PPC blocky image and (33); PSNR = 30.25 dB.

Fig. 7. CLS recovery from the JPEG blocky image and (33); PSNR = 29.68 dB.

Fig. 8. CLS recovery from the JPEG blocky image and (45); PSNR = 29.65 dB.

compression applications because of the popularity of the BDCT. We demonstrated that by the proposed approaches we can reduce the blocking artifacts and simultaneously improve the PSNR distance between the original and recovered images in the decoder. In addition, the proposed approach is general and is not limited only to the BDCT.

The two methods proposed to solve this problem have a number of similarities. First, they are both methods that minimize l_2 metrics. Second, it is easy to see by comparing the projection onto C_2 for a general linear operator Q in (15) and the minimizer of J_a that they both have the same form. Thus, the CLS iterative algorithm can be viewed as a projection algorithm [23]. However, since the parameter μ is kept constant, the size of the smoothness set varies from iteration to iteration. The proposed methods have a number of differentiating features as well. The POCS method offers a more flexible framework than the CLS method in incorporating different types of prior knowledge in the recovery process. However, for the POCS method the definition of certain types of constraint sets used to project onto is not straightforward, as it appears even when the original image is available. For example, we found that if the original image is used to compute the bounds of the sets C_2 and C_2', the resulting sets are very large and contain the blocky image. This problem could be avoided if a normalized smoothness constraint is defined based on the image energy. However, such a set is not convex. In contrast, for the CLS method the regularization parameter μ expresses the tradeoff between two conflicting properties and is measured as a ratio of two weighted l_2 metrics of the desired image. Therefore, its value is normalized and does not depend on the image energy. Thus, the original image can be used to compute values of μ that result in high-quality recovered images.

From a computational point of view, both algorithms converge rapidly, requiring less than 20 iterations. However, the POCS algorithm converges faster, usually requiring less than 10 iterations. This is consistent with the observations in [23], where the relation of the method of successive approximations and projections onto convex sets was examined.

VII. Acknowledgment

The authors acknowledge the contribution of D. Reininger in the early stages of this work [17]. They also acknowledge Dr. H. Stark for his "contagious" enthusiasm in using the theory of POCS for engineering problems.

Appendix A: Derivation of the Projection onto C_2

In the vector space $R^n \times R^n$, a vector is expressed as a two-tuple of vectors in R^n, i.e., $(\boldsymbol{x}, \boldsymbol{y})$, where $\boldsymbol{x}, \boldsymbol{y} \in R^n$. For $(\boldsymbol{x}, \boldsymbol{y}), (\boldsymbol{u}, \boldsymbol{v}) \in R^n \times R^n$, their natural inner product is defined by

$$\langle (\boldsymbol{x}, \boldsymbol{y}), (\boldsymbol{u}, \boldsymbol{v}) \rangle = \langle \boldsymbol{x}, \boldsymbol{u} \rangle + \langle \boldsymbol{y}, \boldsymbol{v} \rangle \qquad \text{(A-1)}$$

where the inner product in the right-hand side is the natural inner product defined in R^n. The inner product defined in (A-1) also induces a norm given by

$$\|(\boldsymbol{x}, \boldsymbol{y})\| = \left[\|\boldsymbol{x}\|^2 + \|\boldsymbol{y}\|^2\right]^{\frac{1}{2}} \qquad \text{(A-2)}$$

where $\|\cdot\|$ in the righthand side is the l_2 norm in R^n.

Define

$$C = \{(\boldsymbol{x}, \boldsymbol{y}) : \|\boldsymbol{x} - \boldsymbol{y}\| \le E, \boldsymbol{x} \in R^n, \boldsymbol{y} \in R^n\}$$

Clearly, C is a subset of the vector space $R^n \times R^n$. It is straightforward to show that set C is closed and convex. Then we have the following:

Lemma 1: For an arbitrary vector $(\boldsymbol{x}, \boldsymbol{y}) \in R^n \times R^n$, the projection $P(\boldsymbol{x}, \boldsymbol{y})$ onto the set C is given by

$$P(\boldsymbol{x}, \boldsymbol{y}) = \begin{cases} (\boldsymbol{x}, \boldsymbol{y}) & \text{if } \|\boldsymbol{x} - \boldsymbol{y}\| \le E \\ (\alpha\boldsymbol{x} + (1-\alpha)\boldsymbol{y}, (1-\alpha)\boldsymbol{x} + \alpha\boldsymbol{y}) & \text{otherwise} \end{cases}$$

where $\alpha = \left[\dfrac{E}{\|\boldsymbol{x} - \boldsymbol{y}\|} + 1\right]/2$.

Proof: By definition, $P(\boldsymbol{x}, \boldsymbol{y})$ is the vector in set C satisfying

$$\|(\boldsymbol{x}, \boldsymbol{y}) - P(\boldsymbol{x}, \boldsymbol{y})\| = \min_{(\boldsymbol{u}, \boldsymbol{v}) \in R^n \times R^n} \|(\boldsymbol{x}, \boldsymbol{y}) - (\boldsymbol{u}, \boldsymbol{v})\|$$

where $(\boldsymbol{x}, \boldsymbol{y}) - (\boldsymbol{u}, \boldsymbol{v}) = (\boldsymbol{x} - \boldsymbol{u}, \boldsymbol{y} - \boldsymbol{v})$, and $(\boldsymbol{u}, \boldsymbol{v}) \in C$.

Clearly, if $(\boldsymbol{x}, \boldsymbol{y}) \in C$, i.e., $\|\boldsymbol{x} - \boldsymbol{y}\| \le E$, then $P(\boldsymbol{x}, \boldsymbol{y}) = (\boldsymbol{x}, \boldsymbol{y})$.

Suppose that $(\boldsymbol{x}, \boldsymbol{y}) \notin C$, then $P(\boldsymbol{x}, \boldsymbol{y})$ can be found by minimizing the Lagrange auxiliary function

$$J_\lambda = \|(\boldsymbol{x}, \boldsymbol{y}) - (\boldsymbol{u}, \boldsymbol{v})\|^2 + \lambda[\|\boldsymbol{u} - \boldsymbol{v}\|^2 - E^2]$$

Taking the gradients of J_λ with respect to vectors $\boldsymbol{u}$ and $\boldsymbol{v}$ and setting them to 0, yields

$$\boldsymbol{u} - \boldsymbol{x} + \lambda(\boldsymbol{u} - \boldsymbol{v}) = 0 \quad \text{and} \quad \boldsymbol{v} - \boldsymbol{y} + \lambda(\boldsymbol{v} - \boldsymbol{u}) = 0,$$

therefore

$$\boldsymbol{u} = \alpha\boldsymbol{x} + (1-\alpha)\boldsymbol{y} \quad \text{and} \quad \boldsymbol{v} = (1-\alpha)\boldsymbol{x} + \alpha\boldsymbol{y}$$

where $\alpha = \dfrac{1+\lambda}{1+2\lambda}$. Furthermore, setting $\|(\boldsymbol{u}-\boldsymbol{v})\| = E$, λ can be found to be $\lambda = \left[\dfrac{\|\boldsymbol{x}-\boldsymbol{y}\|}{E} - 1\right]/2$. ■

Using the above lemma, the projector onto C_2 can be found as follows: Writing the $N \times N$ image f in its column vector form as in (10), the projection of f onto the set C_2 is the $\tilde{f}$ vector in C_2 that minimizes the distance function

$$\|f - \tilde{f}\|^2 = \sum_{i=1}^{N} \|f_i - \tilde{f}_i\|^2 \qquad \text{(A-3)}$$

where $\tilde{f} = \{\tilde{f}_1, \tilde{f}_2, \cdots, \tilde{f}_N\} \in C_2$. In the case of $N = 512$ and 8×8 blocks, Qf is given by (11). Thus, $\|Q\tilde{f}\| \le E$ only constrains columns in the block boundaries.

Define

$$\boldsymbol{x} = \begin{bmatrix} f_8 \\ f_{16} \\ \vdots \\ f_{504} \end{bmatrix} \quad \text{and} \quad \boldsymbol{y} = \begin{bmatrix} f_9 \\ f_{17} \\ \vdots \\ f_{505} \end{bmatrix}$$

Then $Q\tilde{f} = \boldsymbol{x} - \boldsymbol{y}$. It follows immediately from Lemma 1 that the distance function defined in (A-3) is minimized when

$$\tilde{f}_i = \alpha \cdot f_i + (1-\alpha) \cdot f_{i+1}$$
$$\text{and} \quad \tilde{f}_{i+1} = (1-\alpha) \cdot f_i + \alpha \cdot f_{i+1}$$

for $i = 8 \cdot k$ and $k = 1, 2, \cdots, 31$, where $\alpha = \dfrac{1}{2}\left[\dfrac{E}{\|Q \cdot f\|} + 1\right]$; otherwise, $\tilde{f}_i = f_i$. ■

Appendix B: Proof of Propositions 1 and 2

First we prove the following lemma:

Lemma 2: The matrix $A_{(\mu)}$ defined in (26) satisfies the following identities:

1. $A_{(\mu)}\bar{I}_c = \bar{I}_c A_{(\mu)} = \bar{I}_c A_{(\mu)} \bar{I}_c$
2. $A_{(\mu)}^{-1}\bar{I}_c = \bar{I}_c A_{(\mu)}^{-1} = \bar{I}_c A_{(\mu)}^{-1} \bar{I}_c$

and

3. $A_{(\mu)}^{-2}\bar{I}_c = \bar{I}_c A_{(\mu)}^{-2} = \bar{I}_c A_{(\mu)}^{-2} \bar{I}_c$

Proof:

Identity 1: By the definition of $A_{(\mu)}$ in (26), we have

$$A_{(\mu)} = \mu I + \bar{I}_c B S^t S B^t \bar{I}_c.$$

By the idempotent property of $\bar{I}_c$ in (17), we have

$$\begin{aligned} A_{(\mu)}\bar{I}_c &= \left(\mu I + \bar{I}_c B S^t S B^t \bar{I}_c\right)\bar{I}_c \\ &= \mu \bar{I}_c + \bar{I}_c B S^t S B^t \bar{I}_c^2 \\ &= \mu \bar{I}_c + \bar{I}_c^2 B S^t S B^t \bar{I}_c \\ &= \bar{I}_c\left(\mu I + \bar{I}_c B S^t S B^t \bar{I}_c\right) \\ &= \bar{I}_c A_{(\mu)} \end{aligned}$$

Thus we have established the first half of Identity 1: $A_{(\mu)}\bar{I}_c = \bar{I}_c A_{(\mu)}$. Now, applying $\bar{I}_c$ to both sides of the previous equation from the left yields

$$\bar{I}_c A_{(\mu)} \bar{I}_c = \bar{I}_c^2 A_{(\mu)} = \bar{I}_c A_{(\mu)}.$$

Thus, the second half of Identity 1 is shown.

Identity 2: First apply $A_{(\mu)}^{-1}$ to both sides of the first half of Identity 1 from the left; we have

$$\bar{I}_c = A_{(\mu)}^{-1} \bar{I}_c A_{(\mu)}.$$

Then apply $A_{(\mu)}^{-1}$ to both sides of the previous equation from the right,

$$\bar{I}_c A_{(\mu)}^{-1} = A_{(\mu)}^{-1} \bar{I}_c$$

which is the first half of Identity 2. Applying $\bar{I}_c$ to both sides of the previous equation from the left yields the second half of Identity 2.

Identity 3: Identity 3 can be shown using Identity 2. Applying $A_{(\mu)}^{-1}$ to both sides of the first half of Identity 2 from the right yields

$$\bar{I}_c A_{(\mu)}^{-2} = A_{(\mu)}^{-1} \bar{I}_c A_{(\mu)}^{-1}$$

From the first half of Identity 2, we have

$$\bar{I}_c A_{(\mu)}^{-2} = A_{(\mu)}^{-1} A_{(\mu)}^{-1} \bar{I}_c = A_{(\mu)}^{-2} \bar{I}_c$$

which is the first half of Identity 3. The second half directly follows by applying $\bar{I}_c$ to both sides of the previous equation from the right. ■

Lemma 3: The matrix defined by

$$D_\mu = \left(I - A_{(\mu)}^{-1} \bar{I}_c B S^t S B^t \bar{I}_c\right) A_{(\mu)}^{-2}$$

is positive-definite.

Proof: Let $(\lambda_i, \boldsymbol{e}_i)$ denote an eigenvalue and eigenvector pair of the matrix $\bar{I}_c B S^t S B^t \bar{I}_c$. Clearly, $\lambda_i \ge 0$. From the definition of matrix $A_{(\mu)}$, we have

$$A_{(\mu)} \boldsymbol{e}_i = (\mu + \lambda_i)\boldsymbol{e}_i.$$

Hence

$$\begin{aligned} D_\mu \boldsymbol{e}_i &= \left(I - A_{(\mu)}^{-1} \bar{I}_c B S^t S B^t \bar{I}_c\right) A_{(\mu)}^{-2} \boldsymbol{e}_i \\ &= \left(I - A_{(\mu)}^{-1} \bar{I}_c B S^t S B^t \bar{I}_c\right)\left[\frac{1}{(\mu+\lambda_i)^2}\right]\boldsymbol{e}_i \\ &= \frac{1}{(\mu+\lambda_i)^2}\left[\boldsymbol{e}_i - A_{(\mu)}^{-1}(\lambda_i \boldsymbol{e}_i)\right] \\ &= \frac{1}{(\mu+\lambda_i)^2}\left(1 - \frac{\lambda_i}{\mu+\lambda_i}\right)\boldsymbol{e}_i \\ &= \frac{\mu}{(\mu+\lambda_i)^3}\boldsymbol{e}_i \end{aligned}$$

Thus each eigenvector $\boldsymbol{e}_i$ of the matrix $\bar{I}_c B S^t S B^t \bar{I}_c$ is also an eigenvector of the matrix D_μ. Furthermore, the ith

eigenvalue of D_μ is equal to $\frac{\mu}{(\mu+\lambda_i)^3}$ and is positive. Since both matrixes are of the same dimension, it follows that the matrix D_μ is positive-definite. ■

Lemmas 2 and 3 will be used to show Proposition 1. First, consider $J_{S(\mu)}$. Since $A_{(\mu)}$ is symmetric, so is $A_{(\mu)}^{-1}$ from (37), and we have

$$\begin{aligned}\frac{dJ_{S(\mu)}}{d\mu} &= \frac{d}{d\mu}\left\| S\left(I - B^t A_{(\mu)}^{-1}\bar{I}_c BS^t S\right) f' \right\|^2 \\ &= 2\left[S\left(I - B^t A_{(\mu)}^{-1}\bar{I}_c BS^t S\right) f' \right]^t \\ &\quad \cdot \left[S\left(-B^t \frac{dA_{(\mu)}^{-1}}{d\mu}\bar{I}_c BS^t S \right) f' \right].\end{aligned}$$

Since

$$\frac{dA_{(\mu)}^{-1}}{d\mu} = -A_{(\mu)}^{-1}\frac{dA_{(\mu)}}{d\mu}A_{(\mu)}^{-1} = -A_{(\mu)}^{-1}IA_{(\mu)}^{-1} = -A_{(\mu)}^{-2} \tag{B-1}$$

the previous equation yields

$$\begin{aligned}\frac{dJ_{S(\mu)}}{d\mu} &= 2\left[S\left(I - B^t A_{(\mu)}^{-1}\bar{I}_c BS^t S\right) f' \right]^t \left[SB^t A_{(\mu)}^{-2}\bar{I}_c BS^t Sf' \right] \\ &= 2\left[f'^t\left(I - S^t SB^t\bar{I}_c A_{(\mu)}^{-1}B\right) S^t \right] \left[SB^t A_{(\mu)}^{-2}\bar{I}_c BS^t Sf' \right] \\ &= 2f'^t\left(I - S^t SB^t\bar{I}_c A_{(\mu)}^{-1}B\right) S^t SB^t A_{(\mu)}^{-2}\bar{I}_c BS^t Sf' \\ &= 2f'^t\Big(S^t SB^t A_{(\mu)}^{-2}\bar{I}_c BS^t S \\ &\quad - S^t SB^t\bar{I}_c A_{(\mu)}^{-1}BS^t SB^t A_{(\mu)}^{-2}\bar{I}_c BS^t S\Big) f'.\end{aligned}$$

The Identities 2 and 3 in Lemma 2 and the idempotency of $\bar{I}_c$ in (17) further yield

$$\begin{aligned}\frac{dJ_{S(\mu)}}{d\mu} &= 2f'^t\Big(S^t SB^t\bar{I}_c A_{(\mu)}^{-2}\bar{I}_c BS^t S \\ &\quad - S^t SB^t\bar{I}_c A_{(\mu)}^{-1}\bar{I}_c BS^t SB^t\bar{I}_c A_{(\mu)}^{-2}\bar{I}_c BS^t S\Big) f' \\ &= 2f'^t S^t SB^t\bar{I}_c\left(I - A_{(\mu)}^{-1}\bar{I}_c BS^t SB^t\bar{I}_c\right) A_{(\mu)}^2\bar{I}_c BS^t Sf' \\ &= 2f'^t S^t SB^t\bar{I}_c D_\mu\bar{I}_c BS^t Sf'\end{aligned}$$

where D_μ is as defined in Lemma 3.

Consider the vector $\bar{I}_c BS^t Sf'$; in general it is not zero. If it were, the recovered image would always be equal to the blocky image regardless of the value of the regularization parameter μ, as can be seen from (30). Thus, for the general case that $\bar{I}_c BS^t Sf' \neq 0$, Lemma 3 implies that $\frac{dJ_{S(\mu)}}{d\mu}$ is always positive. Therefore, $J_{S(\mu)}$ is a strictly increasing function of μ. ■

Proposition 2 can be proved as follows: From (38) and (B-1), we obtain

$$\begin{aligned}\frac{dJ_{D(\mu)}}{d\mu} &= 2\left[A_{(\mu)}^{-1}\bar{I}_c BS^t Sf' \right]^t \left[\frac{dA_{(\mu)}^{-1}}{d\mu}\bar{I}_c BS^t Sf' \right] \\ &= \left[2A_{(\mu)}^{-1}\bar{I}_c BS^t Sf' \right]^t \left[\left(-A_{(\mu)}^{-2}\right)\bar{I}_c BS^t Sf' \right] \\ &= -2f'^t S^t SB^t\bar{I}_c A_{(\mu)}^{-3}\bar{I}_c BS^t Sf'.\end{aligned}$$

Note that since $A_{(\mu)}$ is positive definite, so is $A_{(\mu)}^{-3}$. Hence for the general case that $\bar{I}_c BS^t Sf' \neq 0$, $\frac{dJ_{D(\mu)}}{d\mu}$ is always negative. Thus, $J_{D(\mu)}$ is a strictly decreasing function of μ. ■

REFERENCES

[1] Committee Draft ISO/IEC CD 10918-1, "Digital compression and coding of continuous-tone still images, part 1: Requirements and guidelines," Mar. 15, 1991.

[2] N. P. Galatsanos and A. K. Katsaggelos, "Methods for choosing the regularization parameter and estimating the noise variance in image restoration and their relation," *IEEE Trans. Image Processing*, vol. 1, no. 3, pp. 322–336, July 1992.

[3] Y. Huang, H. M. Dreizen, and N. P. Galatsanos, "Prioritized DCT for compression and progressive transmission of images," *IEEE Trans. Image Processing*, vol. 1, no. 4, pp. 477–487, Oct. 1992.

[4] B. R. Hunt, "The application of constrained least squares estimation to image restoration by digital computer," *IEEE Trans. Comput.*, vol. 22, pp. 805–812, Sept. 1973.

[5] A. K. Jain, *Fundamentals of Digital Image Processing*. Englewood Cliffs, NJ: Prentice-Hall, 1989.

[6] A. Katsaggelos, J. Biemond, R. M. Mersereau, and R. W. Schafer, "A general formulation of constrained iterative image restoration," in *Proc. ICASSP-85*, Mar. 1985, pp. 700–703.

[7] A. K. Katsaggelos, "Iterative image restoration algorithms," *Opt. Eng.*, vol. 28, pp. 735–748, July 1989.

[8] A. K. Katsaggelos, J. Biemond, R. M. Mersereau, and R. W. Schafer, "A regularized iterative image restoration algorithm," *IEEE Trans. Signal Processing*, vol. 39, pp. 914–929, Apr. 1991.

[9] A. K. Katsaggelos, Ed., *Digital Image Restoration*, Springer Series in Information Sciences, vol. 23. New York: Springer, 1991.

[10] R. L. Lagendijk, J. Biemond, and D. E. Boekee, "Regularized iterative restoration with ringing reduction," *IEEE Trans. Acoust., Speech, Signal Processing*, vol. 36, pp. 1874–1888, Dec. 1988.

[11] H. Musmann, P. Pirsch, and H. Grallert, "Advances in picture coding," *Proc. IEEE*, pp. 523–542, Apr. 1985.

[12] J. M. Ortega and W. C. Rheinboldt, *Iterative Solution of Nonlinear Equations in Several Variables*. New York: Academic, 1970.

[13] T. Ozcelik, J. C. Brailean, and A. K. Katsaggelos, "Recovery of low bit rate compressed images using Gibbs priors," in *Proc. 31st Allerton Conf. Communications, Control and Computing*, Sept. 1993.

[14] B. Ramamurthi and A. Gersho, "Nonlinear space-variant postprocessing of block coded images," *IEEE Trans. Acoust., Speech, Signal Processing*, vol. 34, no. 5, pp. 1258–1267, Oct. 1986.

[15] K. R. Rao and P. Yip, *Discrete Cosine Transform: Algorithms, Advantages, Applications*. New York: Academic, 1990.

[16] H. C. Reeves and J. S. Lim, "Reduction of blocking effects in imaging coding," *Opt. Eng.*, vol. 23, pp. 34–37, Jan./Feb. 1984.

[17] D. Reininger, "Iterative post-processing algorithms for reducing block artifacts in low-bit rate DCT coded images," M.S. thesis, Dep. ECE, Illinois Inst. of Tech. 1991.

[18] P. Santago and S. A. Rajala, "Using convex set techniques for combined pixel and frequency domain coding of time-varying images," *IEEE J. Select. Areas Commun.*, vol. 5, no. 7, pp. 1127–1139, Aug. 1987.

[19] R. W. Schafer, R. M. Mersereau, and M. A. Richards, "Constrained iterative restoration algorithms," *Proc. IEEE*, vol. 69, pp. 432–450, Apr. 1981.

[20] Henry Stark, Ed., *Image Recovery: Theory and Application*. New York: Academic, 1987.

[21] R. L. Stevenson, "Reduction of coding artifacts in transform image coding," in *Proc. ICASSP-93*, Apr. 1993, pp. 401–404.

[22] H. J. Trussell and M. R. Civanlar, "The feasible solution in signal restoration," *IEEE Trans. Acoust., Speech, Signal Processing*, vol. 32, no. 2, pp. 201–212, Apr. 1984.

[23] H. J. Trussell and M. R. Civanlar, "The Landweber iteration and projection onto convex sets," *IEEE Trans. Acoust., Speech, Signal Processing*, vol. 33, pp. 1632–1634, Dec. 1985.

[24] H. Stark and E. T. Olsen, "Projection based image restoration," *J. Opt. Soc. Amer. A*, vol. 9, no. 11, pp. 1914–1919, Nov. 1992.
[25] A. Tikhonov and V. Arsenin, *Solution of Ill-Posed Problems*. New York: Wiley, 1977.
[26] D. C. Youla, "Generalized image restoration by the method of alternating orthogonal projections," *IEEE Trans. Circuits Syst.*, vol. 25, pp. 694–702, Sept. 1978.
[27] D. C. Youla and H. Webb, "Image restoration by the method of convex projections: Part 1—Theory," *IEEE Trans. Med. Imaging*, vol. 1, no. 2, pp. 81–94, Oct. 1982.
[28] R. Rosenholtz and A. Zakhor, "Iterative Procedures for reduction of blocking effects in transform image coding," *IEEE Trans. Circuits Syst. Video Technol.*, vol. 2, no. 1, pp. 91–94, March 1992.

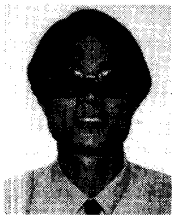

Yongyi Yang was born in Shandong, China, in 1964. He received the BSEE and MSEE degrees from Northern Jiaotong University, Beijing, China, and the MS degree in applied mathematics from Illinois Institute of Technology, Chicago, in 1985, 1988, and 1992, respectively. Currently he is a doctoral candidate in the Department of Electrical and Computer Engineering at Illinois Institute of Technology.

His current research interests are in the general area of signal processing and, more specifically, in signal recovery and image compression.

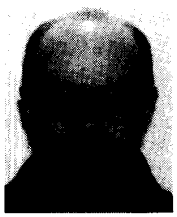

Nikolas P. Galatsanos (S'84–M'85–S'85–M'88–S'89–M'89) was born in Athens, Greece, in 1958. He received the degree in electrical engineering from the National Technical University of Athens, Athens, Greece, in 1982 and the M.S. and Ph.D. degrees in electrical and computer engineering from the University of Wisconsin, Madison, in 1984 and 1989, respectively.

Since August of 1989, he has been on the faculty of the Department of Electrical and Computer Engineering at the Illinois Institute of Technology, Chicago, where he is currently an Assistant Professor. His current research interests include image processing and multidimensional signal processing and, more specifically, recovery and compression of single and multichannel/frame images.

Dr. Galatsanos presently serves as an Associate Editor for the *IEEE Transactions on Image Processing*.

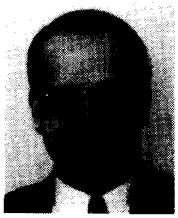

Aggelos K. Katsaggelos (S'80–M'85–SM'92) received the degree in electrical and mechanical engineering from the Aristotelian University of Thessaloniki, Thessaloniki, Greece, in 1979 and the M.S. and Ph.D. degrees in electrical engineering from the Georgia Institute of Technology, Atlanta, in 1981 and 1985, respectively.

In 1985 he joined the Department of Electrical Engineering and Computer Science at Northwestern University, Evanston, IL, where he is currently an Associate Professor. During the 1986–1987 academic year he was an Assistant Professor with the Department of Electrical Engineering and Computer Science, Polytechnic University, Brooklyn, NY. His current research interests include image recovery, processing of moving images (motion estimation and compression), and computational vision.

Dr. Katsaggelos is an Ameritech Fellow and a member of the Associate Staff, Department of Medicine, at Evanston Hospital. He is a member of SPIE, the Steering Committees of the *IEEE Transactions on Medical Imaging* and the *IEEE Transactions on Image Processing*, the IEEE Technical Committees on Visual Signal Processing and Communications and on Image and Multidimensional Signal Processing, the Technical Chamber of Commerce of Greece, and Sigma Xi. He has served as an Associate Editor for the *IEEE Transactions on Signal Processing* (1990–1992), and is currently an Area Editor for the journal *Graphical Models and Image Processing*. He is the editor of *Digital Image Restoration* (New York: Springer, 1991) and the General Chairman of the 1994 Visual Communications and Image Processing Conference (Chicago, IL).